coatings

MDPI

Article

Atomic Layer Deposition of La_2O_3 Film with Precursor La(thd)$_3$-DMEA

Wenyong Zhao, Jie Jiang, Yawen Luo, Jiahao Li and Yuqiang Ding *

International Joint Research Center for Photoresponsive Molecules and Materials, School of Chemical and Material Engineering, Jiangnan University, Wuxi 214122, China
* Correspondence: yding@jiangnan.edu.cn

Abstract: In this paper, a new precursor La(thd)$_3$-DMEA (thd = 2,2,6,6-tetramethyl-3,5-heptanedione, DMEA = N,N′-dimethylethylenediamine) was synthesized and characterized with ^{1}H-NMR and X-ray single crystal diffraction. The thermal properties of La(thd)$_3$-DMEA were checked by thermogravimetric analysis (TGA), which confirmed that the volatility and suitability of La(thd)$_3$-DMEA are suitable for atomic layer deposition (ALD). We studied the atomic layer deposition of La_2O_3 films on a SiO_2 surface with La(thd)$_3$-DMEA and O_3 as precursors. Self-limiting deposition behaviors were found for the prepared films. The purity and surface morphology of the as-grown La_2O_3 films, which possessed a constant growth rate of ~0.4 Å/cycle at 250–280 °C, were confirmed by XPS, SEM, and AFM. The results show that La(thd)$_3$-DMEA is a suitable precursor for the atomic layer deposition of La_2O_3 film.

Keywords: novel lanthanum precursor; mixed ligands; ALD; La_2O_3 film

check for updates

Citation: Zhao, W.; Jiang, J.; Luo, Y.; Li, J.; Ding, Y. Atomic Layer Deposition of La_2O_3 Film with Precursor La(thd)$_3$-DMEA. *Coatings* **2023**, *13*, 870. https://doi.org/10.3390/coatings13050870

Academic Editors: Maxim Yu. Maximov and Yury Koshtyal

Received: 8 April 2023
Revised: 27 April 2023
Accepted: 29 April 2023
Published: 5 May 2023

1. Introduction

In recent years, rare earth metal oxides have garnered considerable attention as high-k dielectric materials due to their potential for high-tech applications [1]. Among various dielectric materials, La_2O_3 has a higher k value (i.e., 27) than those reported for materials such as HfO_2 [2,3], Ta_2O_5 [4,5], Al_2O_3, and others [6–8]. Its high k value makes it suitable for use in metal-oxide-semiconductor field-effect transistors (MOSFETs), catalysis, resistive random-access memory (RRAM), and supercapacitor fields [9–11].

The deposition methods for La_2O_3 dielectrics include metal-organic chemical vapor deposition (MOCVD), physical vapor deposition (PVD), and atomic layer deposition (ALD) [7,12,13]. Among these methods, ALD is considered an attractive technique for obtaining high-quality La_2O_3 films due to its intrinsic self-limiting growth mode. ALD offers several advantages, including the ability to control film thickness by adjusting the number of deposition cycles, low pollution at low deposition temperatures for self-limiting surface reactions, and better film uniformity and conformity compared with other deposition techniques [14–18]. To utilize the benefits of ALD, it is crucial to explore and synthesize new precursors with high volatility and stability.

Numerous studies have investigated lanthanum precursors with different ligands, such as β-diketonate [19], amidinates [20,21], guanidnates [22], and cyclopentadiene (Cp) and its derivatives [23,24], for use in ALD or MOCVD. However, the suitable precursors must possess high volatility and stability. Cyclopentadiene and β-diketonate lanthanum complexes are highly stable and exhibit low volatility, with cyclopentadiene lanthanum complexes being sensitive to water and oxygen. Conversely, the stability of guanidine lanthanum complexes is poor and prone to decomposition. Although β-diketonates have been used as significant ligands for precursors in ALD or MOCVD [25], most lanthanide β-diketonates are polynuclear structures with high melting points and poor volatility, such as La(thd)$_3$ (thd = 2,2,6,6-tetramethylheptane-3,5-dionato), which has a high melting point (238–248 °C) and a high evaporation temperature (180 °C) in ALD [26]. To overcome

these limitations, researchers have focused on developing mixed ligand β-diketonates with different N- and O-donor ligands to improve volatility by increasing the binding force between the lanthanum ion and the neutral ligand. Lanthanide β-diketonate mixed ligand complexes are considered to be the most promising precursors for La_2O_3 film deposition by the ALD technique [27].

Numerous studies have been conducted to develop mixed-ligand β-diketonates with various N- and O-donor ligands. Simon R. Drake et al. [28] synthesized La(thd)$_3$-tetraglyme, which has a low melting point of 41–44 °C, but the tetraglyme was lost during sublimation, resulting in the formation of a dimer. Similarly, Deborah A. et al. [29] synthesized La(thd)$_3$(butyldimethyl-phosphine oxide) as an MOCVD precursor with a melting point of 61–64 °C, but the butyldimethyl-phosphine oxide was also lost. Early studies showed that La(thd)$_3$-Bipy (Bipy = 2,2′-bipyridine) and La(thd)$_3$-Phen (Phen = 1,10-phenanthroline) had decreased volatility due to π-π-stacking interactions, making them unsuitable as precursors. Kang S. W. and Rhee S. W. [30] synthesized La(thd)$_3$-TETEA (TETEA = triethosytriethyleamine), which increased the solubility in *n*-butylacetate and inhibited the polymerization of La(thd)$_3$, leading to separation of the Lewis base at 220 °C. Recently, Nikolaeva et al. synthesized La(thd)$_3$-deda (deda = diethylenetriamine) as an MOCVD precursor that exhibited thermal stability at 140–160 °C [31]. As reviewed above, while previous studies have shown that N-donor neutral ligands have stronger binding forces with lanthanum ions than O-donor neutral ligands [32], the strength of the bond between monoamine and diamine ligands and the lanthanum ion has not been studied. Therefore, the development of mixed ligand complexes of lanthanum dipivaloylmethanates with monoamine and diamine ligands was investigated, which are promising as ALD or CVD precursors.

Three different lanthanum complexes were designed and synthesized. The complexes were characterized using ^{1}H-NMR and X-ray single-crystal diffraction. In addition, their physical and chemical properties, including melting point, thermal stability, volatility, and vapor pressure, were studied using melting point measurements and TGA. To determine their suitability as ALD precursors, the selected complex was used to deposit relevant films through ALD. As the literature reports suggest that ozone (O_3) serves as an efficient source of oxygen for ALD in many metal oxide materials, [33,34], it was selected as the oxidizing agent in the ALD process. The deposition of La_2O_3 was studied in detail, and the composition and surface morphology of the film was analyzed using various techniques.

2. Experimental

2.1. Materials

La(thd)$_3$ was synthesized and characterized using conventional methods, as reported in a previous study [32]. The following chemicals were purchased from Sinopharm Group Chemical Reagent Company and used without further purification: chemically pure $La(NO_3)_3 \cdot 6H_2O$, sodium hydroxide, ethanol, toluene, N,N′-dimethylethylenediamine (DMEA), 2,2,6,6-tetramethyl-3,5-heptanedione (Hthd), dibuthylamine (DBA), and dipropylamine (DPA).

2.2. Instrumentation

NMR spectra were obtained using a Bruker ACF-400 spectrometer (Bruker Company, Fällanden, Switzerland). The melting point of the complex was measured using an X-4A melting point apparatus. The stability and volatility of the complex were investigated using a STA 449 F3 instrument, with a heating rate of 5 °C/min and a temperature range of 20–500 °C.

The structural measurements were conducted using a computer-controlled Oxford Xcalibur E diffractometer (Bruker company, Karlsruhe, Germany), which utilized graphite-monochromated Cu-Ka radiation (λ = 1.54178 Å) at 150(2) K. To correct the data for absorption effects, the multi-scan technique (SADABS) [35] was employed. The structure was solved through the direct method and refined using full-matrix least-squares methods on

F^2, utilizing the SHELXS-97 program package (SHELXS, Bruker AXS Company, Karlsruhe, Germany) [36]. Hydrogen atoms attached to C atoms were considered "riding atoms". Fourier maps were used to locate and refine all non-hydrogen atoms with anisotropic displacement parameters. Hydrogen atoms were positioned based on idealized geometry and refined with fixed isotropic vibration parameters relative to the non-H atoms they were bonded to.

La_2O_3 films were deposited on SiO_2/Si wafers using an ALD reactor (MNT f-100-212, Wuxi, China). The film thickness was measured using an ellipsometer, and the results were calibrated using a Hitachi S-4800 scanning electron microscope (SEM, Helios 600 from Thermo Fisher Scientific, Waltham, MA, USA). The film was post-annealing at 500 °C in a N_2 ambient furnace for 30 min. The composition of the film was explored using the Thermo ESCALAB 250Xi X-ray photoelectron spectroscope (XPS, Theta Probe, Thermo Fisher Scientific Co., Waltham, MA, USA). Additionally, the surface properties of the deposited films were characterized using atomic force microscopy (AFM, XE-100, Park Systems, Suwon, Korea) measurements conducted with a Bruker Dimension Icon.

2.3. Synthesized of La(thd)$_3$ (1)

Based on a previous study [31], La(thd)$_3$ was synthesized as described in Scheme 1. The yield of the sublimed product was 1.301 g (94%), with a melting point of 230.1–235.6 °C. The melting point was consistent with the findings of the previous study [33]. Complex **1** was insoluble in water or dichloromethane, slightly soluble in ethanol, *n*-hexane, and toluene, and soluble in chloroform and N, N′-dimethylformamide.

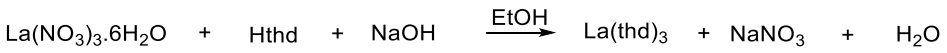

Scheme 1. Synthesis of La(thd)$_3$.

2.4. Synthesized of La(thd)$_3$-DMEA (2)

La(thd)$_3$-DMEA was prepared as described in Scheme 2. To a solution of La(thd)$_3$ (0.413 g, 6 mmol) in 5 mL of toluene under stirring, a solution of DMEA (0.053 g, 6 mmol) in 5 mL of toluene was added dropwise. The mixture was continually stirred for 4 h. After the removal of all volatiles, a white powder was obtained. The powder was then dissolved in 10 mL of 95% hot ethanol and stored at −15 °C for 1 day. White block crystals (0.401 g, 86%) were obtained with a melting point of 125–128 °C. Complex **2** was insoluble in water but was slightly soluble in ethanol and was soluble in most organic reagents such as *n*-hexane and toluene. The ^{1}H NMR spectrum (400 MHz, C_6D_6, 25 °C, ppm) showed signals at δ 5.86 (s, 3H, O=C-CH-C=O), 2.41 (s, 6H, N-CH_3), 2.24 (s, 4H, CH_2), and 1.28 (s, 54H,-CH_3). The ^{13}C NMR spectrum (101 MHz, C_6D_6, 25 °C, ppm) showed signals at δ 197.58 (***C***=O), 89.08 (O=C-***C***H-C=O), 49.85 (-***C***H_2-N), 39.68 (O=C-***C***-), 34.50 (N-***C***H_3), and 27.70 (-***C***H_3).

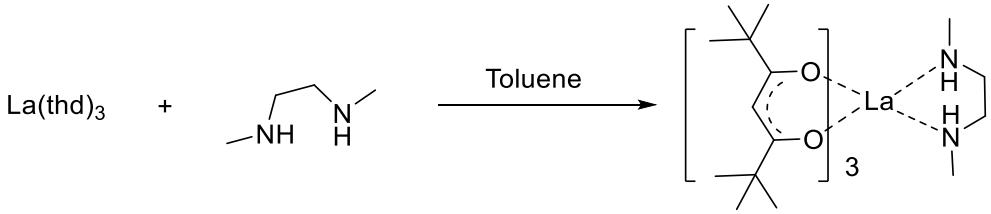

Scheme 2. Synthesis of La(thd)$_3$-DMEA.

2.5. Synthesized of La(thd)$_3$-DBA (3)

Complex **3** was synthesized as described in Scheme 3. La(thd)$_3$ (0.413 g, 6 mmol) was dissolved in 5 mL of hexane under stirring, and then a solution of DPA (0.155 g, 12 mmol) in 5 mL of hexane was added dropwise. The mixture was continuously stirred for 8 h. After the removal of all volatiles to obtain the white powder, the product was dissolved in 5 mL of hexane and stored at −15 °C for 4 h, yielding white block crystals (0.458 g, 80%) with a

melting point of 106–110 °C. The ^{1}H NMR (400 MHz, $CDCl_3$) spectrum exhibited signals at δ 5.64 (s, 3H,O=***CH***-C=O), 2.69–2.49 (m, 8H,NH-***CH$_2$***-CH_2-CH_2-CH_3), 1.48 (q, *J* = 7.8 Hz, 8H, NH-CH_2-***CH$_2$***-CH_2-CH_3), 1.30 (dt, *J* = 14.6, 7.5 Hz, 8H, NH-CH_2-CH_2-***CH$_2$***-CH_3), 1.09 (s, 54H,-C(***CH$_3$***)$_3$), and 0.90 (t, *J* = 7.3 Hz, 12H,CH_2-CH_2-CH_2-***CH$_3$***).

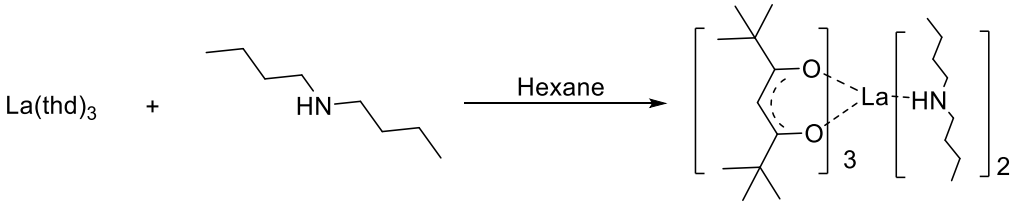

Scheme 3. Synthesis of La(thd)$_3$-DBA.

2.6. Synthesized of La(thd)$_3$-DPA (4)

Complex **4** was synthesized, as described in Scheme 4. La(thd)$_3$ (0.413 g, 6 mmol) was dissolved in 5 mL of *n*-hexane under stirring, and a solution of DPA (0.122 g, 12 mmol) in 5 mL of hexane was added dropwise. The mixture was constantly stirred for 8 h. After the removal of all volatiles, a white powder was obtained. The powder was then dissolved in 5 mL of hexane and stored at −15 °C for 6 h, resulting in the formation of a white power (0.418 g, 78%) with a melting point of 70.4–76.6 °C. The ^{1}H NMR spectrum (400 MHz, $CDCl_3$) exhibited signals at δ 5.64 (s, 3H,O=***CH***-C=O), 2.57 (t, 8H,NH-***CH$_2$***-CH_2-CH_3), 1.63–1.40 (m, 8H, NH-CH_2-***CH$_2$***-CH_3), 1.09 (s, 54H, -C(***CH$_3$***)$_3$), and 0.89 (t, *J* = 7.4 Hz, 12H, CH_2-CH_2-***CH$_3$***).

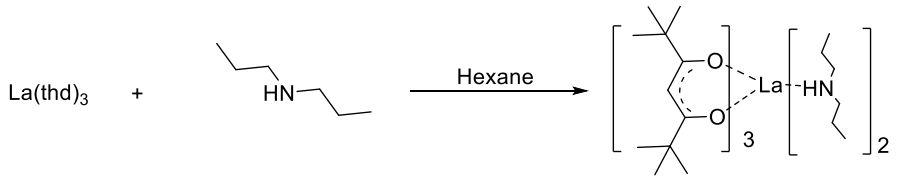

Scheme 4. Synthesis of La(thd)$_3$-DPA.

2.7. Thermogravimetric Analysis

The stability of the complex was investigated using the STA 449 F3 in the temperature range of 20–500 °C, with a heating rate of 5 °C/min in the atmospheric pressure of flowing Ar. The vapor-temperature curve of the complex was obtained based on the Langmuir and Antoine equation using benzoic acid as a standard [37].

2.8. ALD of La_2O_3 Film Details

In this study, La(thd)$_3$-DMEA (**2**) was synthesized and used as the new precursor, and ozone (O_3) was used as the oxygen source. While O_3 was the best choice with the La(thd)$_3$-DMEA, O_3 gas with a volume concentration of approximately 7% in O_2 was generated from oxygen gas (99.999%) using an ozone generator. Prior to film deposition, the organic matter was cleaned using acetone and isopropanol for 10 min each at room temperature, followed by a 30 s rinse in deionized water. Ultra-pure N_2 gas (99.999%) was used as a carrier and purge gas with a flow rate of 200 sccm. The reactor base pressure was approximately 0.3 Torr during N_2 purging. The ALD cycle sequence consisted of O_3 (100 ms)/N_2 (10 s)/La(thd)$_3$-DMEA (8 s)/N_2 (45 s). The La precursor was kept at 150 °C to offer sufficient vapor pressure, producing a vapor pressure of 0.25 Torr/1 atm. However, the film thickness was controlled by adjusting the number of deposition cycles performed within the ALD process window.

3. Result and Discussion

3.1. Crystal Structure Description

The synthesized complexes were characterized using ^{1}H-NMR, ^{13}C-NMR, and X-ray single-crystal diffraction techniques. The proton and carbon signals in both the ^{1}H-NMR and ^{13}C-NMR spectra indicated that complex **2**, complex **3**, and complex **4** were pure. The peaks observed in the ^{1}H-NMR spectrum of complex **2** corresponded to the neutral ligand (DMEA) and the functional groups present in the anionicβ-diketone. The integral ratio of **1:3** for both ligands indicated that the neutral and anionic β-diketones coordinated in a **1:3** ratio. The ^{1}H-NMR spectra of complexes **3** and **4** showed that they were associated with the neutral ligands DPA and DBA, respectively, in a ratio of **2:3**.

Tables 1 and 2 summarize the crystallographic data and structural refinement for complexes **2** and **3**, respectively. To determine the coordination environment of complex **2**, low-temperature solid-state crystalline structure analysis was conducted. Figure 1 and Tables 1 and 2 show the ORTEP diagram, crystallographic data, and selected bond lengths of complex **2**, respectively.

Table 1. Crystal data and structure refinements for complex **2** and **3**.

Paremeters	Complex 2	Complex 3
Empirical formula	$C_{37}H_{69}LaN_2O_6$	$C_{39}H_{93}LaN_2O_6$
Temperature (K)	150	150
Crystal color	clear light colorless	Colorless
Formula weight	776.85	945.16
Crystal system	Monoclinic	Orthorhombic
Space group	$P2_1/c$	$P2_12_12_1$
a (Å)	10.7711(6)	16.7577(14)
b (Å)	26.1684(14)	17.4249(12)
c (Å)	15.5595(10)	18.9628(14)
α (°)	90	90
β (°)	102.455(3)	90
γ (°)	90	90
Volume (Å^3)	4282.4(4)	5537.2(7)
Z	4	4
F(000)	1640	2024
Refinement method	Full-matrix least-squares on F^2	Full-matrix least-squares on F^2
Reflections collection	8440	7760
Independent reflections	7696 (R_{int} = 0.067)	7201 (R_{int} = 0.062)
Range for data collection	3.4–72.2	3.4–59.1
h, k, l range	$-13 \leq h \leq 11$, $-32 \leq k \leq 32$, $-19 \leq l \leq 19$	$-18 \leq h \leq 18$, $-16 \leq k \leq 19$, $-21 \leq l \leq 21$
Goodness-of-fit on F^2	1.106	1.07
Final R indices [I > 2sigma(I^2)]	R = 0.0552, wR_2 = 0.1557	R = 0.0486, wR_2 = 0.1345
R (all data)	R = 0.0584, wR_2 = 0.1594	R = 0.0520, wR_2 = 0.1302

Table 2. Selected bonds lengths (Å) for complex **2** and **3**.

Complex 2		Complex 3	
Bond length	(Å)	Bond length	(Å)
O1—La1	2.448 (3)	La1—O6	2.441 (6)
La1—O4	2.433 (3)	La1—O1	2.443 (6)
La1—O5	2.442 (3)	La1—O3	2.451 (5)
La1—O3	2.450 (3)	La1—O4	2.459 (5)
La1—O2	2.468 (3)	La1—O2	2.463 (5)
La1—O6	2.487 (3)	La1—O5	2.502 (5)
La1—N2	2.756 (5)	La1—N2	2.742 (9)
La1—N1	2.786 (6)	La1—N1	2.783 (10)

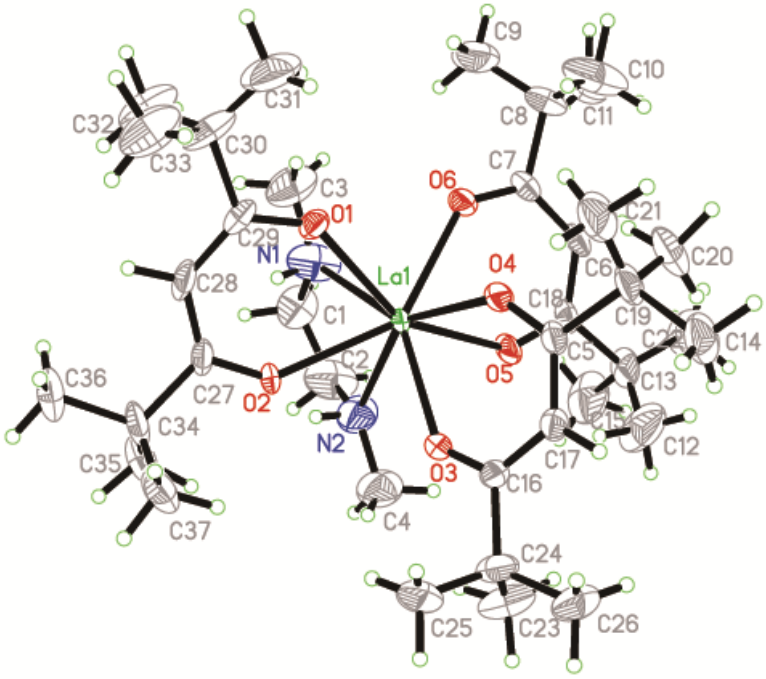

Figure 1. ORTEP diagram of complex **2** showing 30% probability ellipsoids.

The crystal structure of complex **2** was found to be monomeric, and there was no interaction observed between La-La, indicating strong steric shielding of the La nucleus. The La atom was coordinated with six O atoms and two N atoms to form a distorted octahedral geometry through La-O and La-N bonds. The average lengths of La-O and La-N bonds in complex **2** were 2.456 Å and 2.771 Å, respectively, which were similar to the bond lengths found in [La(thd)$_3$(deta)] [31].

The crystal for complex **3** was obtained through the slow crystallization of *n*-hexane. The structure's coordination and crystallographic data are presented in Figure 2 and Table 1. The La atom at the center was coordinated with six O atoms derived from three Hthd ligands and with two N atoms from two Dibuthylamine members, creating a distorted octahedral structure. The La-O bond lengths were comparable to those of complex **2**, synthesized in this study. Based on the crystal structure and ^{1}H NMR data, the structure of the complex appeared reasonable. Although numerous attempts were made, a high-quality crystal of complex **4** could not be obtained, despite its easy solubility in organic solvents such as *n*-hexane. The crystal structure of complex **3** supported the analysis of complex **4** because of the association between the two complexes. Based on the crystal structure and ^{1}H NMR data, the structure of complex **3** appeared reasonable. Additionally, the ^{1}H NMR data of complex **4** demonstrated that its structure conformed to the target product.

3.2. Thermal Behavior of the Lanthanum Precursor

The stability and volatility of precursors are crucial for ALD. Hence, TGA was conducted to study the thermal and volatility properties of complex 2. As shown in Figure 3b, complex **2** exhibited an onset temperature of 249.88 °C for evaporation, with a single-step weight loss. In general, the volatility of precursors can be evaluated by combining the 50% mass loss temperature (T_{50}) and onset temperature, and the relatively lower values of these two parameters for complex **2** (265.7 and 249.88 °C) compared with La(thd)$_3$ (279.27 and 265.84 °C, as seen in Figure 3a,b) indicated that mixed ligands could enhance the volatility of complex **2**. The residue mass of complex **2** after heating up to 501 °C was only 0.32%, demonstrating that complex **2** evaporates almost completely under atmospheric pressure. The DSC curve exhibited one sharp peak at 126 °C and one broad peak at 288 °C. The first event at 126 °C represented the melting of the powder, while the second broad endothermic peak belonged to the complex's evaporation at 288 °C. The TG curve of precursor 2 was

smooth and exhibited only one weightless step, indicating that complex **2** possesses higher stability. It is well-known that the thermal decomposition and volatility of the precursor are critical for ALD.

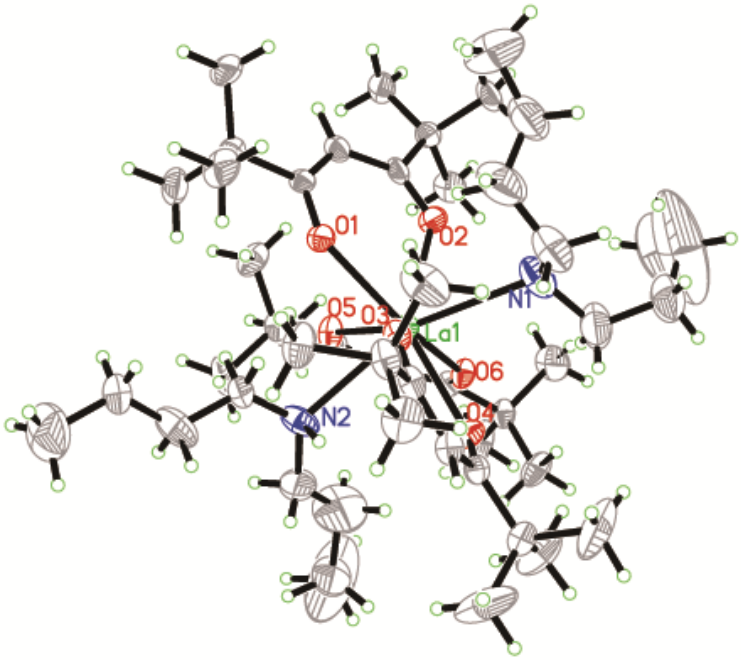

Figure 2. ORTEP diagram of complex **3** showing 30% probability ellipsoids.

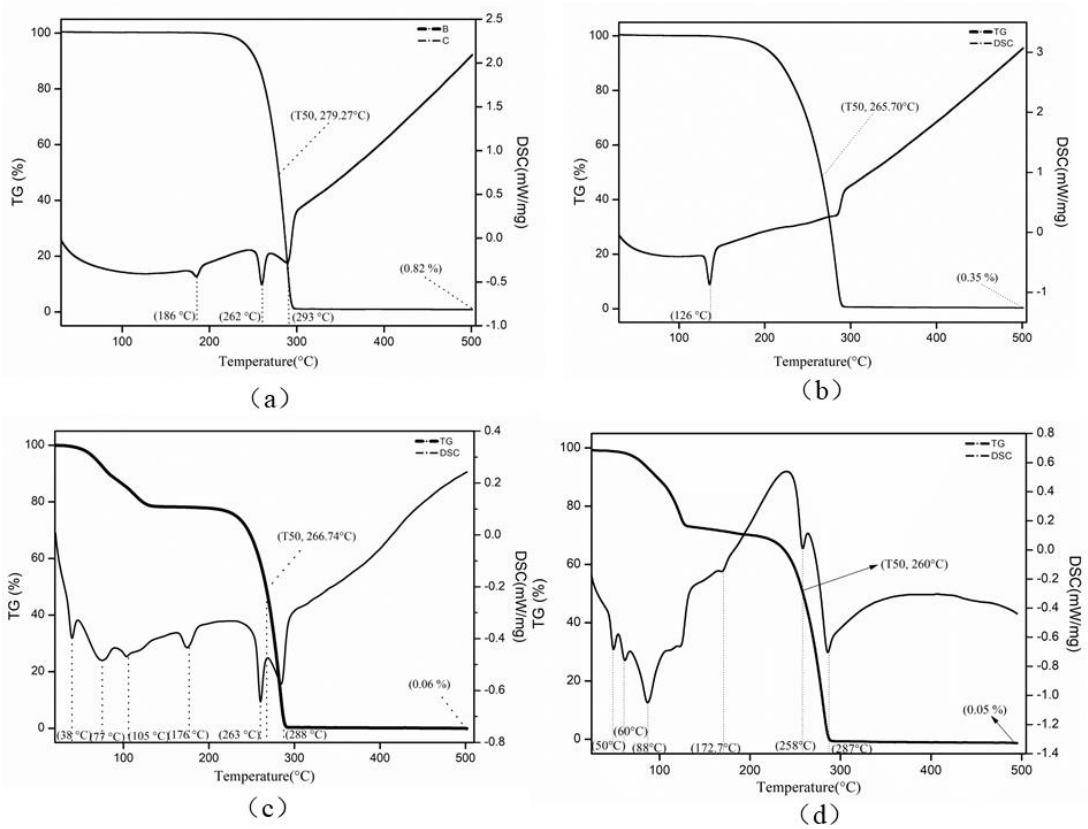

Figure 3. TG/DSC curve of (**a**) complex **1**, (**b**) complex **2,** (**c**) complex **3,** and (**d**) complex **4** in pure N_2.

As shown in Figure 3c, the TG/DSC curve of complex **3** under pre-purified N_2 indicated that the total residue was as low as 0.05%, which declared that the complex almost

completely evaporated under atmospheric pressure. The DSC curve displayed six sharp peaks at 50, 60, 88, 121, 172.7, and 258 °C, as well as one broad peak at 287 °C. The TG curve showed no mass loss at 50, 121, and 172.7 °C, which belonged to some changes in crystals. However, two broad peaks at 60 and 121 °C showed the loss of a member of dibuthylamine. In fact, upon sublimation, complex **3** decomposed with the loss of two members of dipropylamine, resulting in the formation of the homoleptic parent complex **1** at 121 °C. The sixth endothermic peak at 258 °C showed the melting of complex **1** [38], while the broad peak at 287 °C was related to complex **1′**s evaporation.

As shown in Figure 3d, the TG/DSC curve of complex **4** under pre-purified N_2 indicated that the total residue was as low as 0.06%, which declared that the complex almost completely evaporated under atmospheric pressure. The DSC curve displayed five sharp peaks at 38, 77, 105, 176, and 263 °C, as well as one broad peak at 288 °C. The TG curve showed no mass loss at 38, 105, and 176 °C, which belonged to some changes in crystals. However, two broad peaks at 77 and 105 °C showed the loss of a member of dipropylamine. In fact, upon sublimation, complex **4** decomposed with the loss of two members of dipropylamine, resulting in the formation of the homoleptic parent complex **1** at 105 °C. The fifth endothermic peak at 263 °C showed the melting of complex **1** [38], while the broad peak at 288 °C was related to complex **1′**s evaporation. These TG/DSC results demonstrated that the binding force between diamines and lanthanum ions was stronger than that between monoamines and lanthanum ions.

To assess the transport behavior of the precursor and ensure that its flow can be maintained at a suitable level, its vapor pressure is an important factor [39]. In order to determine the evaporation temperature of the precursor, which is also a critical parameter for its delivery, the vapor pressure of complex **2** was evaluated. As shown in Figure 4, complex **2** exhibited a sufficiently high vapor pressure at a low temperature of 130 °C under atmospheric pressure. Specifically, it existed as a liquid with a vapor pressure of approximately 0.1 Torr [40]. Additionally, thermogravimetric analysis (TG) on complex **2** was performed to confirm that it could be maintained at a suitable evaporation temperature during its transfer from the evaporation reactor to the deposition reactor without undergoing thermal decomposition. These results collectively demonstrate that complex **2** meets the requirements of an ALD precursor.

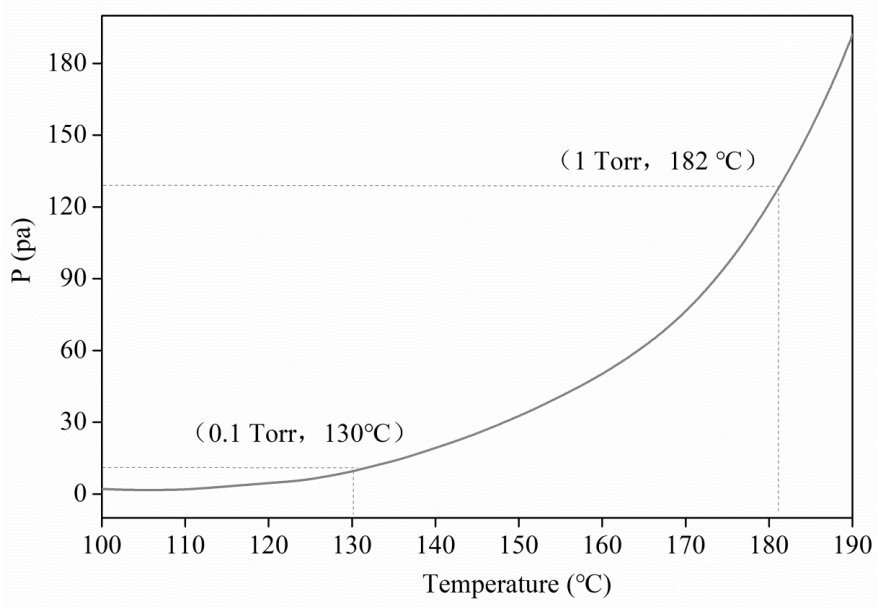

Figure 4. Vapor pressure-temperature curve of complex **2**.

3.3. Growth Characteristics of La_2O_3 Deposition

La_2O_3 film was deposited by an ALD system onto SiO_2/Si(100 wafers. The growth behavior of the La_2O_3 film was investigated by varying the pulse time of complex **2** and ozone precursors. As depicted in Figure 5a,b, the highest growth per cycle of 0.4 Å/cycle was achieved with 8-s La(thd)$_3$-DMEA and 100-ms of ozone pulses. The temperature range was determined and the La_2O_3 films exhibit a nearly stable growth rate of 0.4 Å/cycle, as shown in Figure 5c. The temperature window was found to be between 200–250 °C. However, when the temperature exceeded 270 °C, the growth rate increased abruptly to 0.8 Å/cycle, and the high growth rate at a deposition temperature above 270 °C was attributed to the thermal decomposition of the precursor. Moreover, as illustrated in Figure 5d, the film thickness was found to be linearly related to the number of cycles under the above saturation state, which demonstrated that the growth behavior belongs to the ALD process.

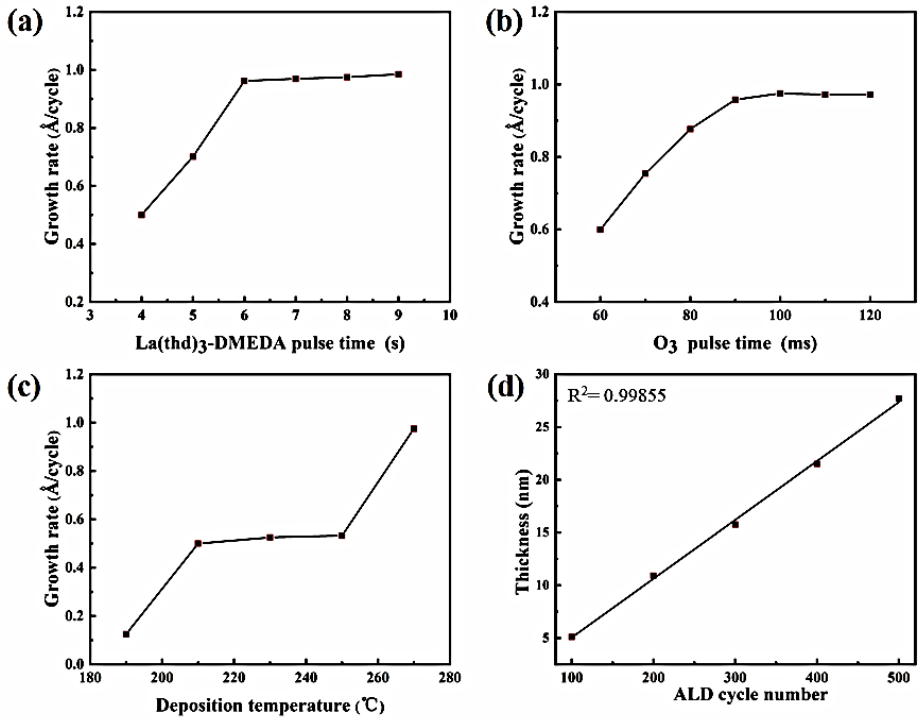

Figure 5. (**a**) Growth rate concerning La(thd)$_3$-DMEA and ozone pulse time; (**b**) growth rate concerning ozone pulse time; (**c**) growth rate at varying deposition temperature for La_2O_3 film; (**d**) film thickness with respect to ALD cycle number.

3.4. Characteristics of La_2O_3 Films

The film thickness, which was used to calculate the growth per cycle, was determined by cross-sectional SEM imaging, as shown in Figure 6a. A 24 nm thick film, grown for 500 ALD cycles at 240 °C, was used for this purpose. The inset of Figure 6a shows the zoomed-in TEM image of the region.

To investigate the morphology of the film, AFM imaging was used, and the result is presented in Figure 6b. The film was continuous and had no cracks. Additionally, the film surface roughness was very low (RMS = 0.671 nm), which indicates that the film had a smooth surface.

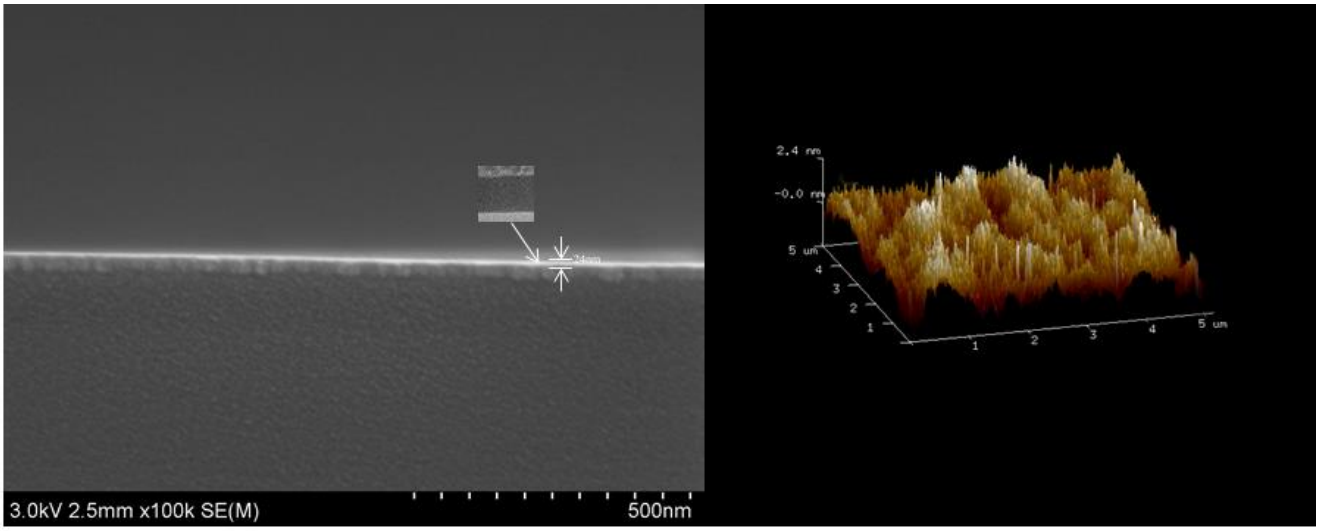

Figure 6. (**a**) Cross-sectional SEM image of a film deposited at 240 °C through 500 ALD cycles, the inset of (**a**) shows the zoomed-in TEM image of the region; (**b**) AFM image of film deposition at 240 °C.

XPS was conducted to investigate the chemical composition of the as-deposited film after Ar^+ sputtering to exclude the surface contamination prior to measurement. Figure 7a shows the survey spectrum of the film grown at 240 °C, which revealed that the major components of the film were La, O, and C. However, after 50 s of Ar^+ sputtering, the C content decreased to 11.67%, indicating that the presented C, which may have been from the air atmosphere, was occasional in Figure 7b. Additionally, the as-grown film also contained a small amount of N, which may have been an ingredient from the precursors, and after sputtering for 50 s, the content of the N element decreased below 2%. As shown in Figure 7c, after the annealing at 500 °C for 30 min, the content of the N element was dramatically decreased to 0.04%. The decrease in the content of the N element with post-annealing may be attributed to densification of the films [41]. Figure 8 shows the high-resolution La3d and O1s XPS spectra of the film. As shown in Figure 8a, the spectral lines of La3d were recorded at 830.3–860.3 eV. The doublet peaks of 833.2 and 837.6 eV correspond to $La3d_{5/2}$, while the doublet peaks of 850.0 and 854.6 eV belong to $La3d_{3/2}$ [42]. The four peaks confirm the formation of La_2O_3. In Figure 8b, the peak located at 532.0 eV, which corresponds to the La-OH species, was significantly reduced by 50 s of Ar^+ sputtering, revealing that most of the La-OH components were distributed on the surface of the film and formed due to exposure to air. In addition, the XPS spectrum of the film after sputtering was not analyzed, because Ar^+ may lead to changes in the composition of the film [43]. Undoubtedly, the results showed that the synthesized complex **2** could deposit La_2O_3 films used as an ALD lanthanum precursor.

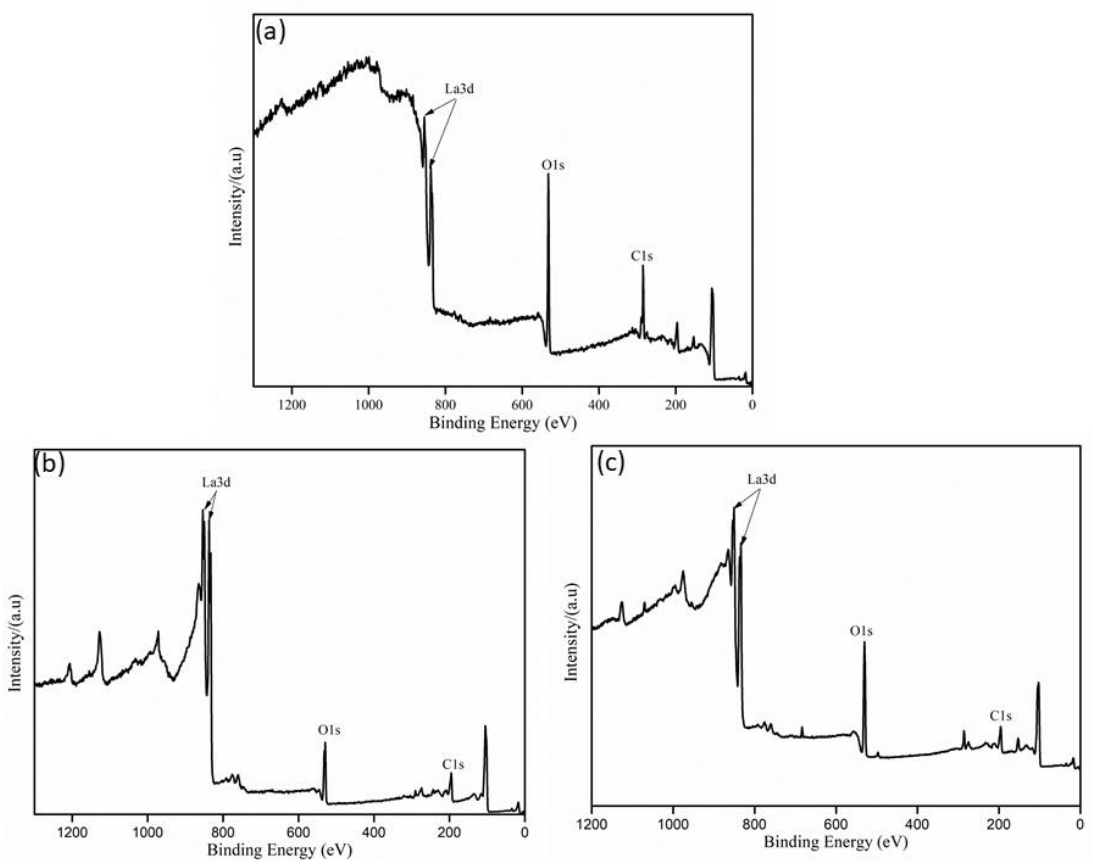

Figure 7. XPS survey spectra of a film deposited at 240 °C: (**a**) as deposited; (**b**) after sputtering for 50 s; (**c**) post-annealing at 500 °C for 30 min in N_2 ambient furnace.

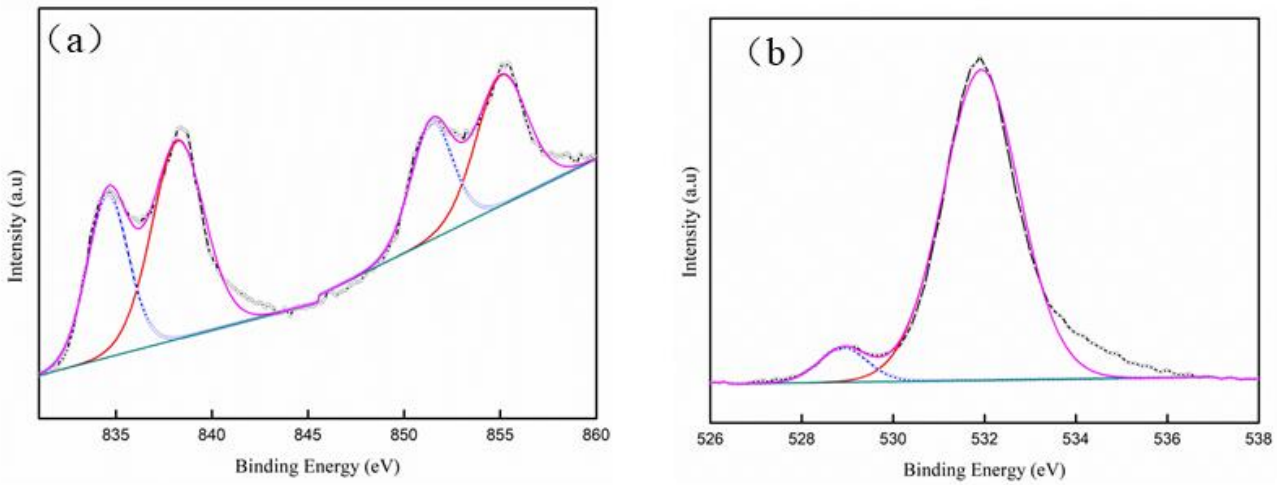

Figure 8. High-resolution XPS spectra of La 3d and O 1s regions of films deposited at 240 °C: (**a**,**b**) as deposited. Purple and red lines represent smooth curves; the blue line represents the baseline.

The above analysis indicated that the deposition of the La_2O_3 film on the SiO_2/Si substrate was successful, and complex **2** proved to be a suitable potential ALD precursor.

4. Conclusions

In conclusion, the introduction of neutral ligands can depolymerize the polymer into monomers, reduce the melting point, and improve the volatility of the complex. Moreover, the complexing ability of a nitrogen-containing bidentate ligand with a lanthanum ion

is stronger than that of a nitrogen-containing monodentate ligand. ^{1}H-NMR and X-ray single-crystal diffraction results proved that the structure of complex **2** was consistent with the target structure. The thermogravimetric analysis and vapor pressure results show that the volatility and suitability of La(thd)$_3$-DMEA are suitable for ALD. La(thd)$_3$-DMEA and ozone were used as precursors to successfully deposit La_2O_3 film on the SiO_2 surface by ALD. A remarkable growth rate of ALD La_2O_3 of up to 0.4 Å/cycle in the temperature range of 200–250 °C was achieved. All the analyses show that La(thd)$_3$-DMEA is a suitable potential ALD precursor.

Author Contributions: Conceptualization, Y.D.; methodology, J.J.; software, Y.L. and J.L.; formal analysis, Y.L. and J.L.; writing—original draft preparation, W.Z.; writing—review and editing, W.Z. All authors have read and agreed to the published version of the manuscript.

Funding: This research received no external funding.

Institutional Review Board Statement: Not applicable.

Informed Consent Statement: Not applicable.

Data Availability Statement: Not applicable.

Conflicts of Interest: The authors declare no conflict of interest.

References

1. Kim, W.H.; Maeng, W.J.; Moon, K.J.; Myoung, J.M.; Kim, H. Growth characteristics and electrical properties of La_2O_3 gate oxides grown by thermal and plasma-enhanced atomic layer deposition. *Thin Solid Films* **2010**, *519*, 362–366. [CrossRef]
2. Xiao, M.; Qiu, C.; Zhang, Z.; Peng, L.M. Atomic-layer-deposition growth of an ultrathin HfO_2 film on graphene. *ACS Appl. Mater. Interfaces* **2017**, *9*, 34050–34056. [CrossRef]
3. Dong, H.; Brennan, B.; Zhernokletov, D.; Kim, J.; Hinkle, C.L.; Wallace, R.M. In situ study of HfO_2 atomic layer deposition on InP (100). *Appl. Phys. Lett.* **2013**, *102*, 171602-1–171602-4. [CrossRef]
4. Egorov, K.V.; Lebedinskii, Y.Y.; Markeev, A.M.; Orlov, O.M. Full ALD Ta_2O_5-based stacks for resistive random access memory grown with in vacuo XPS monitoring. *Appl. Surf. Sci.* **2015**, *356*, 454–459. [CrossRef]
5. Wang, X.; Liu, H.; Zhao, L.; Fei, C.; Feng, X.; Chen, S.; Wang, Y. Structural properties characterized by the film thickness and annealing temperature for La_2O_3 films grown by atomic layer deposition. *Nanoscale Res. Lett.* **2017**, *12*, 233. [CrossRef] [PubMed]
6. Jinesh, K.B.; Lamy, Y.; Wolters, R.A.; Klootwijk, J.H.; Tois, E.; Roozeboom, F.; Besling, W.F.A. Silicon out-diffusion and aluminum in-diffusion in devices with atomic-layer deposited La_2O_3 thin films. *Appl. Phys. Lett.* **2008**, *93*, 192912. [CrossRef]
7. Popovici, M.I.; Walke, A.M.; Bizindavyi, J.; Meersschaut, J.; Banerjee, K.; Potoms, G.; Kostantine, K.; Bosch, G.V.D.; Delhougne, R.; Kar, G.S.; et al. High-endurance ferroelectric (La, Y) and (La, Gd) Co-doped hafnium zirconate grown by atomic layer deposition. *Acs. Appl. Electron. Mater.* **2022**, *4*, 1823–1831. [CrossRef]
8. Fan, J.; Liu, H.; Li, D.; Wang, S.; Duan, L.; Yu, X. Interfacial thermal stability and band alignment of La_2O_3/Al_2O_3 nanolaminates deposited by atomic layer deposition. *J. Mater. Sci.-Mater. Electron.* **2017**, *28*, 11253–11259. [CrossRef]
9. Chen, L.; Yang, W.; Li, Y.; Sun, Q.Q.; Zhou, P.; Lu, H.L.; Zhang, D.W. Resistive switching properties of plasma enhanced-ALD La_2O_3 for novel nonvolatile memory application. *J. Vac. Sci. Technol. A* **2012**, *30*, 01A148-1–01A148-4. [CrossRef]
10. Onn, T.M.; Gathmann, S.R.; Guo, S.; Solanki, S.P.S.; Walton, A.; Page, B.J.; Rojas, G.; Neurock, M.; Grabow, L.C.; Mkhoyan, K.A.; et al. Platinum Graphene Catalytic Condenser for Millisecond Programmable Metal Surfaces. *J. Am. Chem. Soc.* **2022**, *144*, 22113–22127. [CrossRef]
11. Edelmann, F.T. Lanthanide amidinates and guanidinates in catalysis and materials science: A continuing success story. *Chem. Soc. Rev.* **2012**, *41*, 7657–7672. [CrossRef]
12. Devi, A. 'Old Chemistries' for new applications: Perspectives for development of precursors for MOCVD and ALD applications. *Coord. Chem. Rev.* **2013**, *257*, 3332–3384. [CrossRef]
13. Oh, I.K.; Kim, M.K.; Lee, J.S.; Lee, C.W.; Lansalot-Matras, C.; Noh, W.; Kim, H. The effect of La_2O_3-incorporation in HfO_2 dielectrics on Ge substrate by atomic layer deposition. *Appl. Surf. Sci.* **2013**, *287*, 349–354. [CrossRef]
14. Agrawal, K.S.; Barhate, V.N.; Patil, V.S.; Patil, L.S.; Mahajan, A.M. Plasma-enhanced atomic layer-deposited La_2O_3 ultra-thin films on Si and 6H-SiC: A comparative study. *Appl. Phys. A-Mater.* **2020**, *126*, 650. [CrossRef]
15. Fei, C.; Liu, H.; Wang, X.; Fan, X. The influence of process parameters and pulse ratio of precursors on the characteristics of $La_{1-x}Al_xO_3$ films deposited by atomic layer deposition. *Nanoscale Res. Lett.* **2015**, *10*, 180. [CrossRef] [PubMed]
16. Kouda, M.; Suzuki, T.; Kakushima, K.; Ahmet, P.; Iwai, H.; Yasuda, T. Electrical properties of CeO_2/La_2O_3 stacked gate dielectrics fabricated by chemical vapor deposition and atomic layer deposition. *Jpn. J. Appl. Phys.* **2012**, *51*, 121101-1–121101-5. [CrossRef]
17. George, S.M. Atomic Layer Deposition: An Overview. *Chem. Rev.* **2010**, *110*, 111–131. [CrossRef]
18. Mackus, A.J.M.; Bol, A.A.; Kessels, W.M.M. The use of atomic layer deposition in advanced nanopatterning. *Nanoscale* **2014**, *6*, 10941–10960. [CrossRef]

19. Sawka, A. Metal-organic chemical vapour deposition of lanthana-doped ceria layers at low temperatures. *Ceram. Int.* **2021**, *47*, 5198–5208. [CrossRef]
20. Chen, P.Y.; Hadamek, T.; Kwon, S.; Al-Quaiti, F.; Posadas, A.B.; Kim, M.J.; Ekerdt, J.G. Role of template layers for heteroepitaxial growth of lanthanum oxide on GaN(0001) via atomic layer deposition. *J. Vac. Sci. Technol. A* **2020**, *38*, 012403-1–012403-8. [CrossRef]
21. Lou, X.; Gong, X.; Feng, J.; Gordon, R. Band offset analysis of ALD La_2O_3 on GaAs (111), (110) and (100) surfaces for epitaxial growth. *ACS Appl. Mater. Inter.* **2019**, *11*, 28515–28519. [CrossRef]
22. Qian, C.; Zhang, X.; Li, J.; Xu, F.; Zhang, Y.; Shen, Q. Trisguanidinate lanthanide complexes: Syntheses, structures, and catalytic activity for mild amidation of aldehydes with amines. *Organometallics* **2009**, *28*, 3856–3862. [CrossRef]
23. Endo, K.; Kato, K.; Takenaka, M.; Takagi, S. Electrical characteristic of atomic layer deposition La_2O_3/Si MOSFETs with ferroelectric-type hysteresis. *Jpn. J. Appl. Phys.* **2019**, *58*, SBBA05-1–SBBA05-5. [CrossRef]
24. Suzuki, T.; Kouda, M.; Ahmet, P.; Iwai, H.; Kakushima, K.; Yasuda, T. La_2O_3 gate insulators prepared by atomic layer deposition: Optimal growth conditions and MgO/La_2O_3 stacks for improved metal-oxide-semiconductor characteristics. *J. Vac. Sci. Technol. A* **2012**, *30*, 01A148-1–01A148-4. [CrossRef]
25. Mao, X.; Foucher, A.C.; Stach, E.A.; Gorte, R.J. Changes in Ni-NiO equilibrium due to $LaFeO_3$ and the effect on dry reforming of CH_4. *J. Catal.* **2020**, *381*, 561–569. [CrossRef]
26. Eisentraut, K.J.; Sievers, R.E. Volatile Rare Earth Chelates. *J. Am. Chem. Soc.* **1965**, *87*, 5254–5256. [CrossRef]
27. Stafford, N.A.; Katamreddy, R.; Guerin, L.; Feist, B.; Dussarrat, C.; Pallem, V.; Opila, R. Atomic layer deposition of rare-earth oxide thin films for high-k dielectric applications. *ECS Trans.* **2009**, *19*, 525–536. [CrossRef]
28. Alexandra, M.Z. Lanthanide β-diketonate glyme complexes exhibiting unusual co-ordination modes. *J. Chem. Soc. Dalton Trans.* **1993**, *15*, 2379–2386.
29. Neumayer, D.A.; Purtell, R.J.; Kane, W.F.; Grill, A. Preparation of (PB, LA)TIO_3 films by metal organic chemical vapor deposition with new lanthanum precursors. *Integr. Ferroelectr.* **1997**, *14*, 85–93. [CrossRef]
30. Kang, S.W.; Rhee, S.W. Deposition of La_2O_3 films by direct liquid injection metallorganic chemical vapor deposition. *J. Electrochem. Soc.* **2002**, *149*, C345–C348. [CrossRef]
31. Nikolaeva, A.; Nygaard, R.; Martynova, I.; Tsymbarenko, D. Synthesis, structure and thermal behavior of volatile mononuclear mixed ligand complexes of rare-earth dipivaloylmethanates with diethylentriamine. *Polyhedron* **2020**, *180*, 114373. [CrossRef]
32. Nemukhin, A.V.; Rogachev, A.Y.; Konyukhov, S.V.; Bochenkova, A.V.; Granovsky, A.A. QM/MM modeling of the structures and properties of the β-diketonate-based lanthanide complexes. *Int. J. Quantum Chem.* **2005**, *104*, 203–213. [CrossRef]
33. Ahn, S.; Littlewood, P.; Liu, Y.; Marks, T.J.; Stair, P.C. Stabilizing supported Ni catalysts for dry reforming of methane by combined La doping and Al overcoating using atomic layer deposition. *ACS Catal.* **2022**, *12*, 10522–10530. [CrossRef]
34. Lamagna, L.; Wiemer, C.; Perego, M.; Volkos, S.N.; Baldovino, S.; Tsoutsou, D.; Fanciulli, M. O_3-based atomic layer deposition of hexagonal La_2O_3 films on Si(100) and Ge(100) substrates. *Am. J. Phys.* **2010**, *108*, 084108-1–084108-10. [CrossRef]
35. Sheldrick, G.M. *SHELXS-97, Program for Crystal Structure Solution*; University of Göttingen: Göttingen, Germany, 1997.
36. Sheldrick, G.M. *SHELXL-97, Program for Crystal Structure Refinement*; University of Göttingen: Göttingen, Germany, 1997.
37. Wright, S.F.; Dollimore, D.; Dunn, J.G.; Alexander, K. Determination of the vapor pressure curves of adipic acid and triethanolamine using thermogravimetric analysis. *Thermochim. Acta* **2004**, *421*, 25–30. [CrossRef]
38. Li, X.L.; Tsoutsou, D.; Scarel, G.; Wiemer, C.; Capelli, S.C.; Volkos, S.N.; Fanciulli, M. Chemical and structural properties of atomic layer deposited La_2O_3 films capped with a thin Al_2O_3 layer. *J. Vac. Sci. Technol. A* **2009**, *27*, L1–L7. [CrossRef]
39. Du, L.; Wang, K.; Zhong, Y.; Liu, B.; Liu, X.; Ding, Y. A high growth rate process of ALD CeO_x with amidinato-cerium [(N-^{i}Pr-AMD)$_3$Ce] and O_3 as precursors. *J. Mater. Sci.* **2020**, *55*, 5378–5389. [CrossRef]
40. Bedoya, C.; Condorelli, G.G.; Finocchiaro, S.T.; Di Mauro, A.; Atanasio, D.; Fragala, I.L.; Carella, S. MOCVD of Lanthanum Oxides from La(tmhd)$_3$ and La(tmod)$_3$ Precursors: A Thermal and Kinetic Investigation. *Chem. Vap. Depos.* **2006**, *12*, 46–53. [CrossRef]
41. Park, N.K.; Kang, D.K.; Kim, B.H.; Jo, S.J.; Ha, J.S. Electrical properties of La_2O_3 thin films grown on TiN/Si substrates via atomic layer deposition. *Appl. Surf. Sci.* **2006**, *252*, 8506–8509. [CrossRef]
42. Barhate, V.; Agrawal, K.; Patil, V.; Patil, S.; Mahajan, A. Spectroscopic study of La_2O_3 thin films deposited by indigenously developed plasma-enhanced atomic layer deposition system. *Int. J. Mod. Phys. B* **2018**, *32*, 1840074-1–1840074-5. [CrossRef]
43. Zhang, Y.; Du, L.; Liu, X.; Ding, Y. A high growth rate atomic layer deposition process for nickel oxide film preparation using a combination of nickel (II) diketonate–diamine and ozone. *Appl. Surf. Sci.* **2019**, *481*, 138–143. [CrossRef]